



Optimization of Intense Pulsed Light Sintering Considering Dimensions of Printed Cu Nano/Micro-paste Patterns for Printed Electronics

Yong-Rae Jang¹ · Chung-Hyeon Ryu¹ · Yeon-Taek Hwang¹ · Hak-Sung Kim^{1,2}

Received: 7 June 2019 / Revised: 3 December 2019 / Accepted: 6 December 2019 / Published online: 12 February 2020
© Korean Society for Precision Engineering 2020

Abstract

An intense pulsed light (IPL) was irradiated for the sintering of screen-printed copper (Cu) nano/micro-paste patterns on a polyimide substrate. The pattern widths and intervals affect the sintering behavior owing to the opto-thermal relationship during IPL irradiation. The temperature histories of the patterns during the IPL sintering process were predicted using a self-developed heat transfer simulation program. By comparing the experimental and simulation results, the tendency according to the size of the Cu pattern was confirmed. At the same IPL irradiation energy, the wider the pattern and the narrower the interval between the patterns, the higher the heat generated. To demonstrate the tendency, in situ resistance monitoring of the Cu patterns was conducted and their microscopic structures were investigated using a scanning electron microscope. Through the tendency of IPL sintering according to the widths and intervals of the Cu pattern, guidelines of IPL sintering process for electrodes with multi-size pattern were suggested: A dummy pattern was added between the existing digitizer patterns to achieve uniform sintering in all regions. When IPL sintering was conducted with the dummy patterns, the uniformly sintered line resistance could be obtained in entire areas of the digitizer pattern.

Keywords Pattern width and interval · IPL sintering · Heat generation · Copper nano/micro pattern · Printed electronics

1 Introduction

The flexible printed circuit board (FPCB) market has been gradually increased in various areas. FPCBs have conventionally been fabricated through a photolithography process. However, such processing is expensive and inefficiently long owing to complicated steps such as cleaning, preparation, exposure, and etching. By contrast, the printed electronics process is cost-effective and convenient owing to its simple three-step approach (printing, sintering, and inspection).

Various applications such as flexible displays [1–3], flexible organic light-emitting diodes (OLED) [4, 5], flexible solar cells [6, 7], radio frequency identification tags (RFID)

[8, 9], wearable electronics [10, 11], and flexible touch screens [12, 13] can be produced using printed electronics technology. The fabrication of a conductive pattern is one of the most important aspects of printed electronics. To fabricate a conductive pattern, metal nanoparticle pastes, such as gold (Au) and silver (Ag), have been widely used owing to their high conductivity and oxidation stabilities. However, such materials are too expensive for commercialization [14, 15]. To overcome these disadvantages, copper (Cu) nanoparticle ink or paste has been used to fabricate an FPCB conductive pattern owing to its low cost and high conductivity.

There is a need for a process capable of sintering each other to achieve better conductivity. There are various methods for this process, including thermal [16], laser [17, 18], plasma [19], microwave [20, 21], NIR [22], and IPL sintering. However, Cu particles are easily oxidized by oxygen, moisture, and high temperature. Owing to these weaknesses, conventional thermal sintering process cannot be used. Other methods have the disadvantage of expensive equipment and complicated processes. Therefore, the use of the intense pulsed light (IPL) sintering process was first introduced and patented in 1969 [23]. After 33 years, IPL

✉ Hak-Sung Kim
kima@hanyang.ac.kr

¹ Department of Mechanical Engineering, Hanyang University, 17 Haengdang-Dong, Seongdong-Gu, Seoul 133-791, South Korea

² Institute of Nano Science and Technology, Hanyang University, Seoul 133-791, South Korea

sintering with nanoparticle ink was reported again in two patents by Miyashita et al. and Hirai et al. [24, 25]. The IPL sintering processes of Cu nanoparticles were further investigated by other groups. Various factors such as solvent, pH, and reductant concentration have been explored in detail and optimized in order to produce a nanoparticle ink at room temperature by Ruvini et al. [26]. Furthermore, Patil et al. demonstrate a simple, convenient and low cost synthesis method for Cu nanoparticles through the reduction of copper salt in ethylene glycol using rongalite as novel reducing agent as well as capping agent and IPL sintering technique used to archive conductive electrode pattern for printing electrode [27]. In addition, Araki et al. confirmed that the ratio of the carbon/Cu determined the light absorbance coefficients which are the most important factors in IPL sintering [28]. There was also an attempt to fabricate green electrodes using cellulose nanocrystals (CNC), graphene nanoplatelets (GNP) and copper precursors via IPL sintering process [29]. Schroder et al. introduced a commercial IPL machine [30, 31]. Also, in our previous studies, it was reported that the oxide shell could be removed through a photo thermal reaction with a polymer binder such as poly (N-vinylpyrrolidone) (PVP) and ethyl cellulose (EC) during IPL sintering process [32–34].

For higher electrical conductivity and sintering properties, IPL sintering of mixed Cu particles has been studied with various sizes of copper particles. To reduce the material cost and reduce the pores for better packing density, the mixed Cu nano-/micro-inks with different ratios of Cu nano/micro particles were fabricated and sintered by IPL irradiation [35]. A bimodal Cu nano-ink with 25:75 wt % case (40 nm:100 nm Cu NPs) sintered by multi-pulse IPL irradiation exhibited the lowest resistivity and the highest adhesion strength (5B adhesion level), which is due to the high density of the Cu micro structure [36]. On the other hand, Abdullah et al. found a correlation between the proportion of two different sized particles and the packing density and porosity of the paste [37]. They used the 2 μm micro-particle with the 180 nm nanoparticles to increase the electrical conductivity and reduce the material price. According to Abdullah et al.'s study, the ratio of large particles to entire particles should be theoretically about 2/3 to minimize the porosity when the dimension ratio of each particle is 11.11 (equal to 2 μm /180 nm). Therefore, in this work, a copper nano/micro paste was prepared by mixing proper sizes of Cu particles at an optimum ratio (180 nm particles: 2 μm particles = 1:1.4).

The IPL sintering process of the copper paste was closely related the preparation conditions such as the screen-printing speed and drying temperature. The printing speed influences the printability by determining the shear rate and viscosity of the paste [38, 39], and the drying temperature affects the removal of residual solvents and binders and the oxidation of copper particles [40]. In

addition, not only IPL irradiation conditions (e.g. pulse duration [41], frequency, pulse number, irradiation energy) but also external conditions (e.g. UV irradiation [36, 40], wavelength of IPL [42, 43], heating and vacuuming [44], etc.) were closely related to the IPL sintering characteristics. However, in all the previous studies, only uniform printed patterns were printed and sintered. In order to develop larger, thinner and curved electronic devices, different sized patterns should be printed and sintered on one substrate. However, a study on the characteristics of IPL sintering of the different sized patterns is not conducted yet to the author's best knowledge. In this work, we found that the sintering characteristics can change remarkably with different sizes of the pattern such as widths and intervals under the same sintering process conditions (100 mm/s printing speed, 100 °C NIR drying for 10 min, a single pulse, 5 J/cm² of energy, and a 5-ms duration) (Fig. 1). This phenomenon can cause resistance uniformity problems in applications with multi-size patterns.

Therefore, in this study, the IPL sintering characteristics with respect to various pattern widths and intervals were investigated through an analytical and experimental approach. The heat generation by the IPL irradiation was predicted according to the widths and intervals of the pattern using a self-developed program named 'FLS program'. The macrostructures and microstructure of the sintered patterns were also observed and compared using an optical microscope and a scanning electron microscope (SEM). Based on these results, we predicted the tendency of IPL sintering according to the sizes of Cu patterns and proceeded the uniform sintering of digitizer application with multi-sized pattern.

2 Experiment and Simulation

2.1 Fabrication of Cu Nano/Micro-paste

For the fabrication of the Cu nano/micro-paste, commercial Cu nanoparticles (NPs) (180 nm in diameter; Ning-Guangbo) (10 g) and Cu micro particles (MPs) (2 μm in diameter; JoinM) (14 g) were used. The mixing ratio of 1:1.4 (NPs:MPs) was selected based on the reference for higher packing density [37]. The Cu nano/micro particles were dispersed in a mixed solvent of diethylene glycol butyl ether (DEGBE, $\geq 99\%$; Sigma Aldrich) (1.85 g), ethylene glycol (EG, 99.8%; Sigma Aldrich) (e1 g), α -terpineol (80.0%; Tokyo Chemical Industry Co., Ltd.), and polymer binders of ethyl cellulose (EC, $\geq 49.0\%$; Sigma Aldrich) (0.15 g), Poly urethane diol (PUD, 88 wt % in H₂O; Sigma Aldrich) (Table 1). The mixed Cu nano/micro-paste was dispersed using an ultrasonicator for 3 h and a 3-roll-mill for 1 h.

Different sintering results

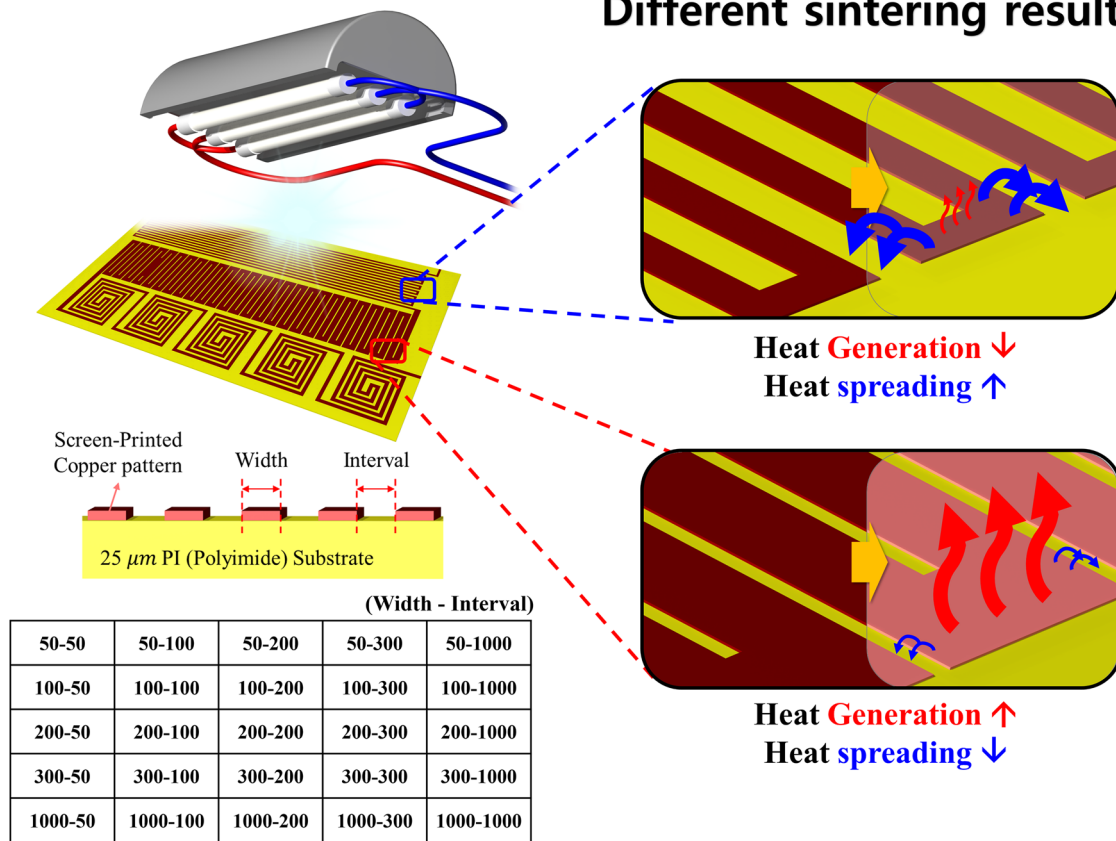


Fig. 1 Printed Cu nano/micro pattern with respect to the pattern widths (50, 100, 200, 300, and 1000 μm) and intervals (50, 100, 200, 300, and 1000 μm)

Table 1 Properties of the copper electrode, PI substrate and aluminum plate for simulate the flash light sintering process

Properties	Copper electrode	PI substrate	Aluminum plate
Heat capacity (J/kg K)	384	1090	902
Thermal conductivity (W/m k)	401	0.4	237
Density (kg/m ³)	8940	1420	2700
Thickness (μm)	10	25	5000

2.2 Preparation of Cu Nano/Micro-paste Pattern

To investigate the sintering characteristics of the Cu nano/micro-paste pattern with respect to the dimensions of the printed patterns (width and interval), the screen plate was designed to print various pattern dimensions classified by the pattern width (50, 100, 200, 300, and 1000-μm) and pattern interval (50, 100, 200, 300, and 1000-μm). To demonstrate the effect of the Cu nano/micro pattern dimensions on the IPL sintering, ten columns of each pattern were arrayed horizontally (Fig. 1). The fabricated Cu nano/micro-paste was printed onto PI substrates (SKC Kolon PI) with a 25-μm thickness using a screen printer (Tiger SP2825-MT; Daeyoung HighTech Co.) at a printing speed of 100 mm/s. The printed Cu nano/micro-paste patterns were dried using the

near infrared (NIR) wavelength range (800–1500 nm, at 500 W; Adphos L40) for 10 min at 100 °C.

2.3 IPL Sintering of Cu Nano/Micro-paste Pattern with Respect to the Pattern Dimensions

The printed Cu nano/micro-paste patterns were sintered using IPL irradiation from three xenon lamps (maximum recommended power of 4.5 kW water-cooled, wavelength of 350–950 nm; First light Lamps, Ltd.). The IPL irradiated from xenon lamps was reflected using a large area reflector, which can uniformly cover an area of 110 mm × 130 mm. The sintering process was applied at room temperature and under ambient conditions. In this study, the IPL irradiation energy was varied from 4 to 6 J/cm², whereas other IPL

irradiation conditions, such as the number of pulses (1) and pulse duration (5 ms), were fixed. The irradiation energy of the IPL was measured using a power meter (Nova II; Ophir Optonics Solutions, Ltd.)

2.4 Heat Transfer Simulation Using Finite Difference Numerical Calculation Method

To predict the temperature history of a Cu pattern during IPL irradiation, a heat transfer simulation was conducted.

An analytical model was deduced for the finite difference method calculation, as shown in Fig. 2. According to the heat transfer theory [45], a general two-dimensional finite difference formulation of the heat conduction in implicit method can be expressed as follows:

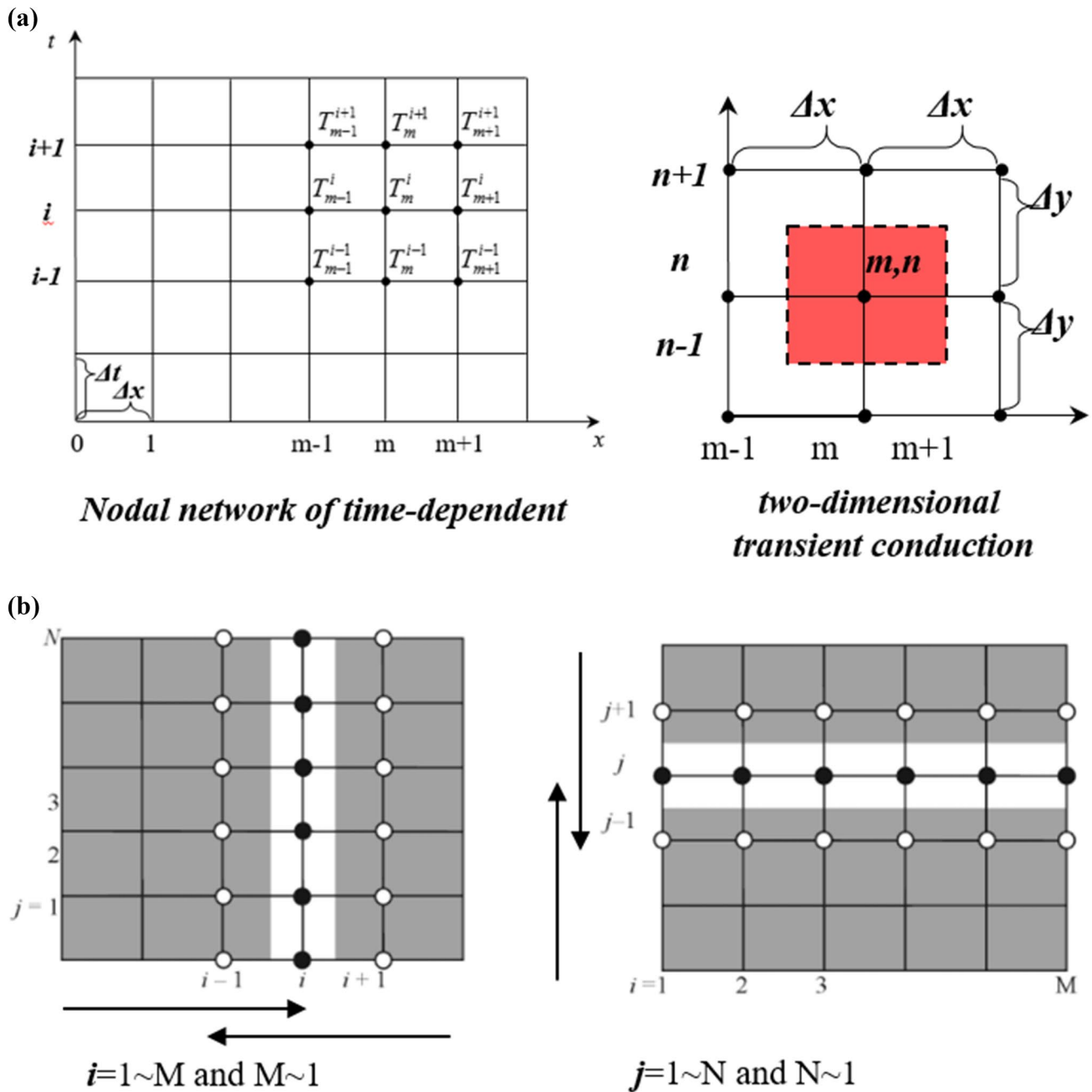


Fig. 2 Schematic figure of **a** two-dimensional based finite difference analysis and **b** line-by-line tridiagonal matrix algorithm (TDMA) method

$$k\Delta y \frac{T_{m-1,n}^{i+1} - T_{m,n}^{i+1}}{\Delta x} + k\Delta x \frac{T_{m,n+1}^{i+1} - T_{m,n}^{i+1}}{\Delta y} + k\Delta y \frac{T_{m+1,n}^{i+1} - T_{m,n}^{i+1}}{\Delta x} + k\Delta x \frac{T_{m,n-1}^{i+1} - T_{m,n}^{i+1}}{\Delta y} + \dot{q}_{m,n}\Delta x\Delta y = \rho\Delta x\Delta yC \frac{T_m^{i+1} - T_m^i}{\Delta t} \tag{1}$$

where k , C , and ρ are the thermal conductivity, specific heat capacity, and density, respectively. Subscripts m and n are the x - and y -direction node locations, and T^i is the temperature at time i . In the original equation, there was a term related to the internal heat generation rate \dot{q} , but since there was no heat source inside the copper pattern, \dot{q} became 0 and this term was deleted. This equation can be simplified as follows:

$$T_{left}^{i+1} + T_{top}^{i+1} + T_{right}^{i+1} + T_{bottom}^{i+1} - 4T_{node}^i = \frac{T_{node}^{i+1} - T_{node}^i}{\tau} \tag{2}$$

$$\tau = \alpha\Delta t/l^2, \quad \alpha = k/\rho C, \quad l = \Delta x = \Delta y$$

The time-dependent transient heat conduction formulation is calculated using an implicit method. This is because an explicit method requires an extremely small time-step and takes a long time to calculate such finite difference formulations [46, 47]. For this reason, an implicit method with relatively stable computations and a large time-step was used. Using this implicit method to solve the unknown temperature variables at time $i + 1$, a numerical calculation

of the tridiagonal matrix algorithm (TDMA) was conducted as follows:

$$\mathbf{Ax} = \mathbf{d} \tag{3}$$

$$\begin{bmatrix} b_1 & c_1 & & & 0 \\ a_2 & b_2 & c_2 & & \\ & a_3 & b_3 & \ddots & \\ & & \ddots & \ddots & c_{n-1} \\ 0 & & & a_n & b_n \end{bmatrix} \begin{bmatrix} x_1 \\ x_2 \\ x_3 \\ \vdots \\ x_n \end{bmatrix} = \begin{bmatrix} d_1 \\ d_2 \\ d_3 \\ \vdots \\ d_n \end{bmatrix} \tag{4}$$

where \mathbf{A} and \mathbf{d} denote the $n \times n$ and $n \times 1$ constant matrix, respectively, and \mathbf{x} is an $n \times 1$ unknown matrix. This TDMA method was applied to n nodes of each vertical line, allowing a line-by-line ($n \times m$) TDMA calculation to be conducted. As shown in Fig. 3, a 3×3 TDMA calculation can be expanded to an $n \times n$ TDMA calculation. An FLS simulation was conducted using Microsoft Visual Studio 2015 and National Instrument LabVIEW 2015 software based on the 2D finite difference model.

2.5 Characterization

To measure the electrical conductivity of the Cu nano/micro-paste pattern, their sheet resistance and thickness were measured using a 4-point probe method (1- μm -diameter probe tip, 1-mm probe tip interval; Modusystems, Inc.) with a source meter (2015 THD, Keithley) and an alpha step (KLA Tencor AS500, Tencor instruments). Furthermore, to investigate the

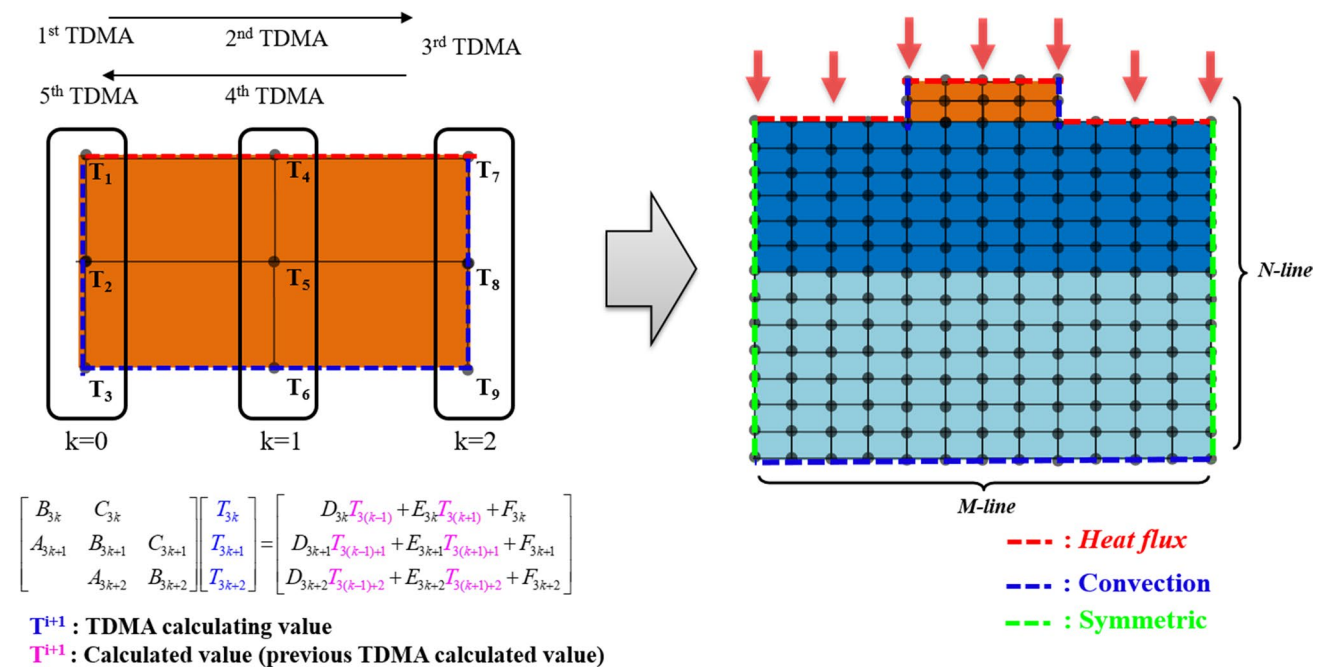


Fig. 3 3x3 TDMA calculation method and expanded 2D finite difference model calculated by line-by-line ($N \times M$) TDMA method

sintering process with respect to the pattern dimensions, an in situ resistance monitoring was conducted while a IPL was irradiated onto the patterns. The in situ resistance monitoring system was composed of a Wheatstone bridge circuit, a source meter, and an oscilloscope. The microstructures of the Cu nano/micro-paste patterns were observed using a scanning electrode microscope (SEM, S4800; Hitachi) with a 15 kV operating voltage.

3 Results and Discussion

3.1 Results on IPL Sintering Experiments

An IPL pulse with a fixed irradiation condition (a single pulse, 5-ms pulse duration, and 5 J/cm^2 of irradiation energy) was irradiated onto the various sizes of Cu nano/micro patterns. The irradiation of the IPL caused surface plasmonic resonance, and the electrons in the Cu particles were vibrated and generated heat [48–50]. The polymer binders were decomposed and removed by the generated heat [34]. During this occurrence, the Cu oxide shell was removed with the decomposition of the polymer binder. In addition, the generated heat created a necking between the Cu nanoparticles, connecting them [41].

Figure 4a shows the resistivity of the IPL sintered Cu patterns according to the pattern intervals and widths at an

irradiation energy of 5 J/cm^2 . It was noteworthy that the resistivity of the specimens after the IPL sintering under the same irradiation energy and conditions decreased as the width of the patterns widened and the interval narrowed. Figure 5a–e shows the sintered Cu patterns according to their intervals with a fixed width of $50\text{-}\mu\text{m}$, which were observed using an optical microscope. Please note that this is the $50\text{-}\mu\text{m}$ width row case shown in Fig. 4a. The Cu pattern with a $50\text{-}\mu\text{m}$ width and $50\text{-}\mu\text{m}$ interval sintered by IPL irradiation showed a resistivity of $31.05 \mu\Omega \text{ cm}$. The Cu pattern with a $50\text{-}\mu\text{m}$ width with wider widths of $1000\text{-}\mu\text{m}$ had the lowest resistivity to $11.36 \mu\Omega \text{ cm}$. By contrast, the Cu pattern with a $50\text{-}\mu\text{m}$ width with wider intervals of $1000\text{-}\mu\text{m}$ had the highest resistivity to $44.75 \mu\Omega \text{ cm}$. This indicates that the resistivity of the Cu pattern decreased as the interval narrowed and the width widened.

To observe the microstructure of the Cu pattern, a scanning electron microscope (SEM) analysis was conducted (Fig. 5f–k). Before IPL irradiation, the Cu micro-particles and nanoparticles were covered with a Cu oxide shell and a polymer binder layer (Fig. 5k), which interfered with the electrical current flow through the particles. After the IPL irradiation (Fig. 5f–j), the polymer binder and oxide shell covering the Cu particles were removed through the instant heat generated during the IPL sintering, which is similar to previous studies [34, 41, 51]. As shown in the SEM images of Fig. 5f, the coalescence among the particles during the

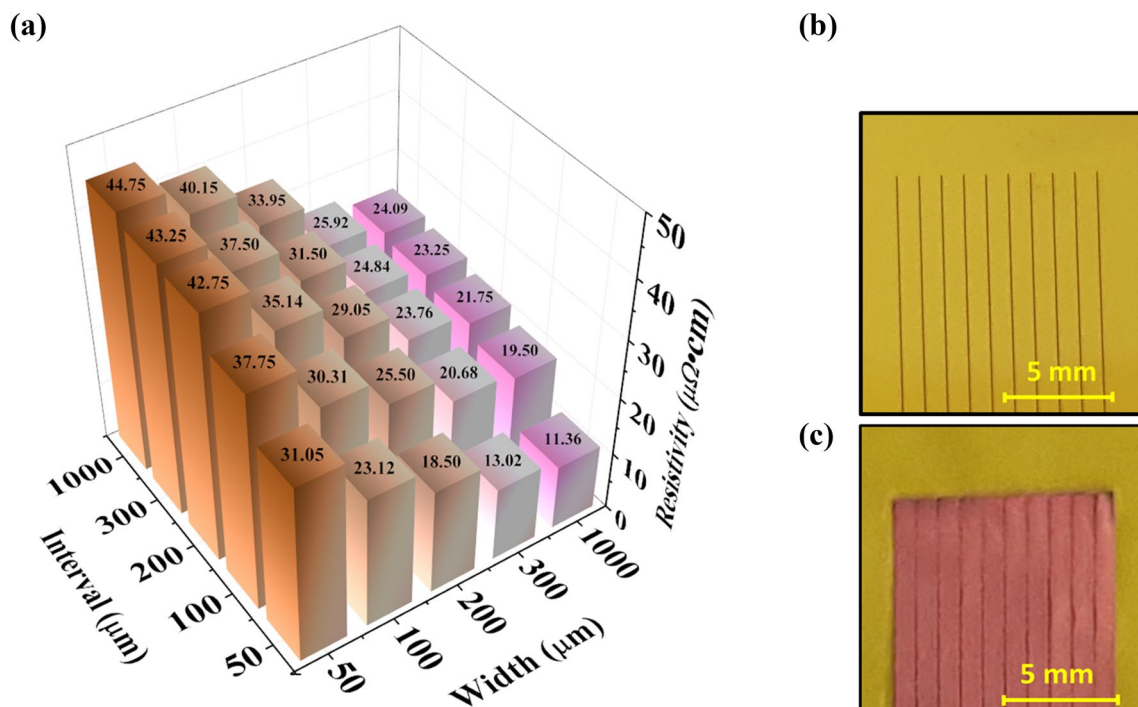


Fig. 4 a Resistivity of the Cu patterns with respect to their widths and intervals after IPL sintering with irradiation energy of 5 J/cm^2 . b The specimen with the width of $50 \mu\text{m}$ and interval of $1000 \mu\text{m}$. c The specimen with the width of $1000 \mu\text{m}$ and interval of $50 \mu\text{m}$

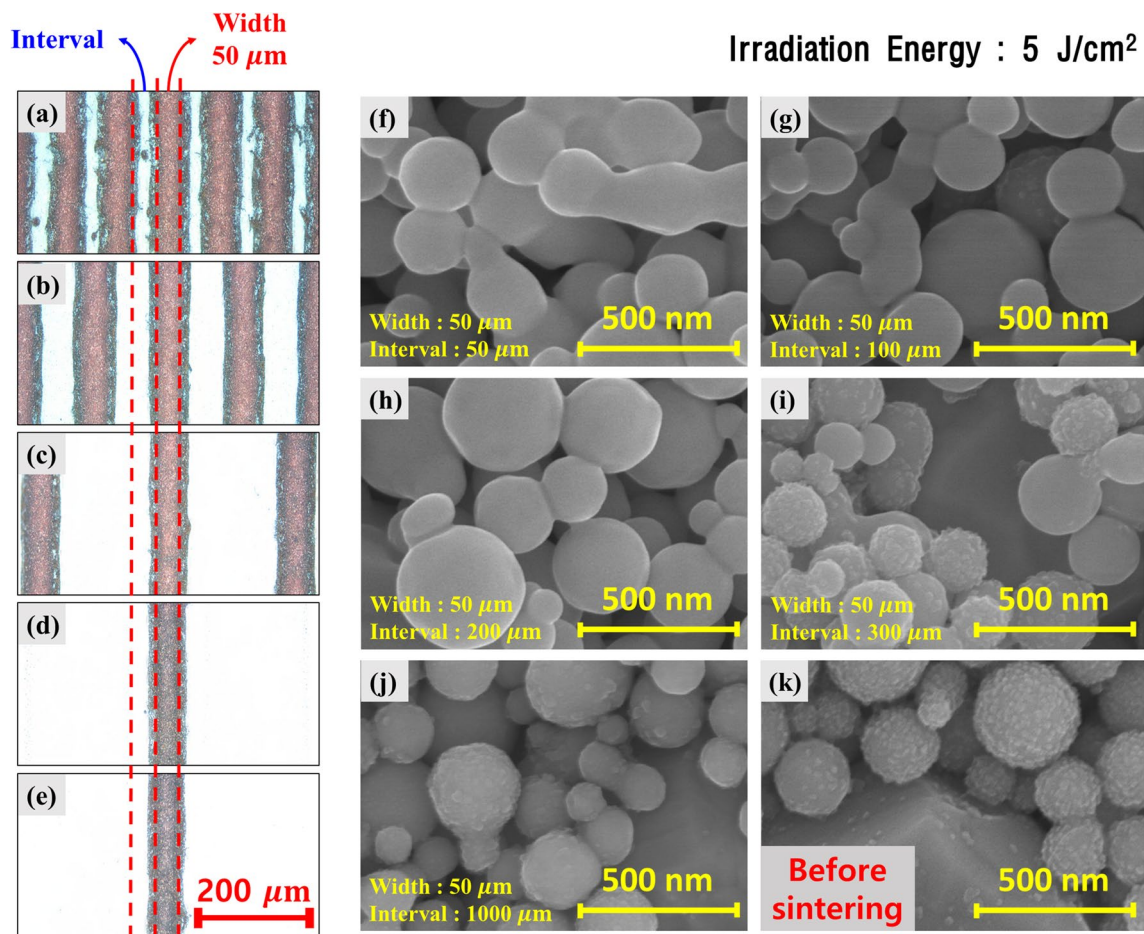


Fig. 5 The Cu patterns with the width of 50 μm and the intervals of **a** 50 μm , **b** 100 μm , **c** 200 μm , **d** 300 μm , **e** 1000 μm which were sintered by IPL irradiation of same energy (5 J/cm^2) and observed with optical microscope. The Scanning Electron Microscope (SEM)

IPL irradiation was well formed in the case of the 50- μm pattern interval. Meanwhile, necking junctions among the particles were not sufficiently formed in the case of the 1000- μm pattern interval (see the SEM images of Fig. 5j). From Fig. 5f–j, it can be concluded that the necking between the particles was denser as the interval narrowed, which contributed to its lower resistivity.

On the other hand, Fig. 6a–e shows the sintered Cu patterns according to their various widths with a fixed interval of 50- μm , as shown using an optical microscope. In the SEM images of the microstructures for each case (Fig. 6f–j), it was found that the sintering of the Cu particles during the IPL irradiation was noticed as the width of the patterns widened, which resulted in a lower resistivity. As shown in Fig. 6j, where the pattern width was the widest (1000- μm) and the interval was the narrowest (50- μm), Cu nanoparticles were sintered together by melting junction between each particles. In the case of 1000–50 case, because the width of the pattern is wide, it is difficult to escape the heat generated between

images of the copper pattern with the width of 50 μm and the intervals of **f** 50 μm , **g** 100 μm , **h** 200 μm , **i** 300 μm , **j** 1000 μm which were sintered by IPL irradiation of same energy (5 J/cm^2). **K** The SEM image of the Cu pattern before IPL sintering

the particles. Also, because the interval of the pattern is narrow, the cooling through the substrate is very small and the temperature may increase significantly.

3.2 Results on Heat Transfer Simulations

To investigate the reason for the different sintering phenomena according to the pattern dimensions, an analytical heat transfer simulation of the Cu paste pattern was conducted using the FLS program. IPL irradiation conditions same as the experiments were entered into the program. In addition, the properties of the Cu pattern, PI substrate, and aluminum plate shown in Table 1 were used. As shown in Fig. 7, the temperatures were rapidly increased immediately after the IPL irradiation at 5 J/cm^2 . When the interval of the Cu pattern was wider than 200- μm , there were no noticeable differences in the maximum temperature. By contrast, it was found that when the interval of the Cu pattern was decreased from 200 to 50- μm , the maximum temperature

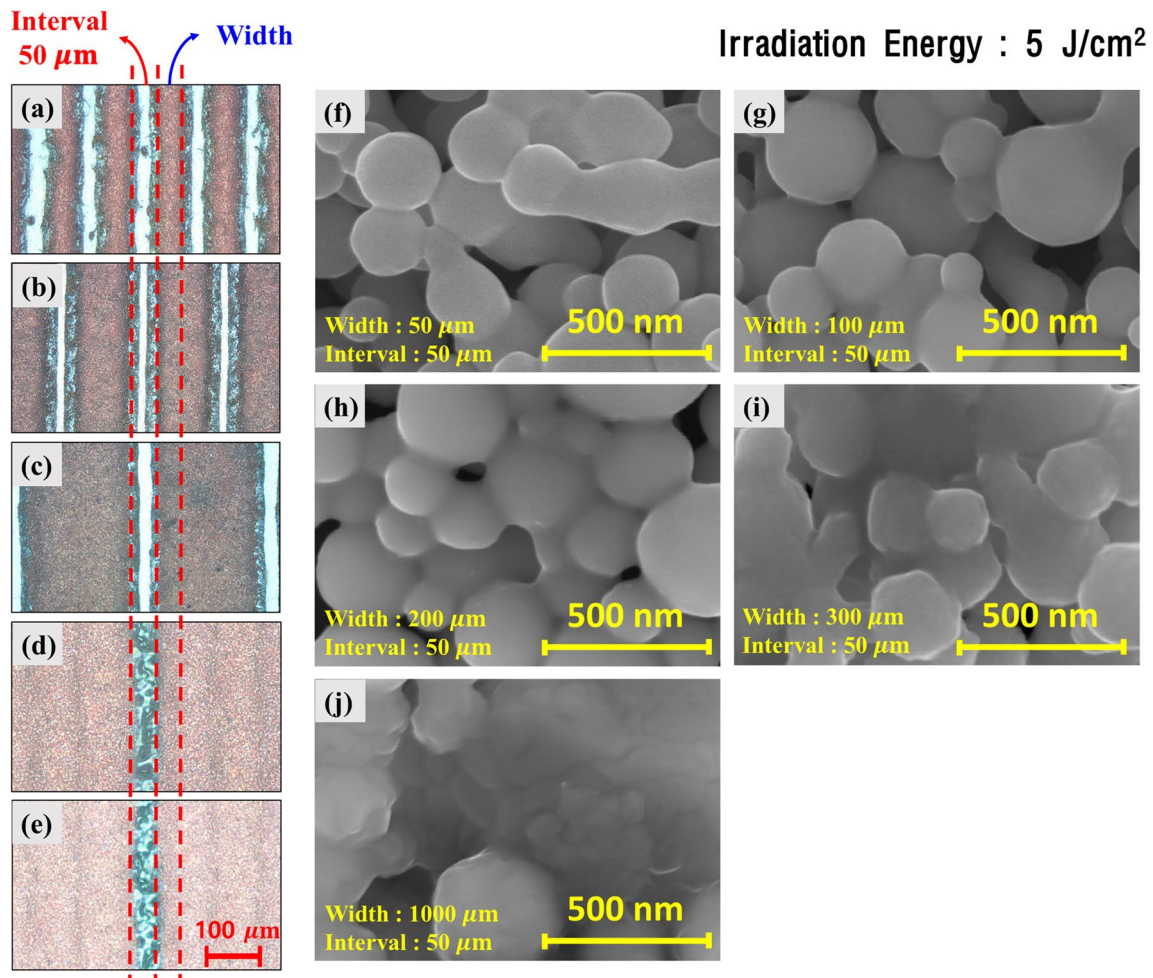


Fig. 6 The Cu patterns with the interval of 50 μm and the widths of **a** 50 μm , **b** 100 μm , **c** 200 μm , **d** 300 μm , **e** 1000 μm which were sintered by IPL irradiation of same energy (5 J/cm^2) and observed with optical microscope. The Scanning Electron Microscope (SEM)

images of the copper pattern with the interval of 50 μm and the widths of **f** 50 μm , **g** 100 μm , **f** 200 μm , **i** 300 μm , **j** 1000 μm which were sintered by IPL irradiation of same energy (5 J/cm^2)

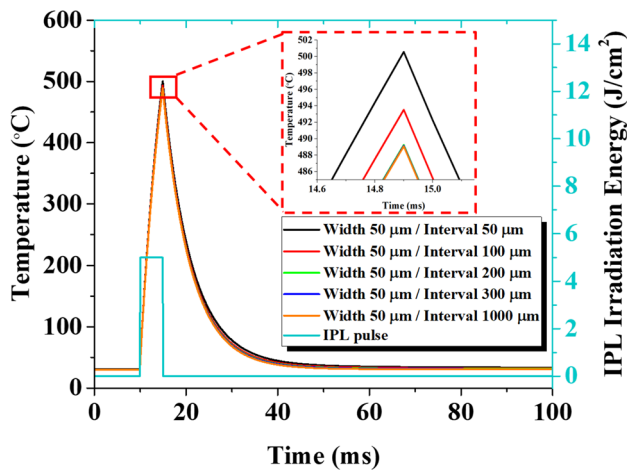


Fig. 7 Temperature distributions of the Cu patterns which have same width of 50 μm and different intervals (50, 100, 200, 300, 1000 μm)

was remarkably increased. As the interval of the pattern decreased from 1000 to 50- μm , the maximum temperature increased from 489.1 to 500.6 $^{\circ}\text{C}$ (see the inset in Fig. 7).

The temperature history was also calculated using the FLS program (Fig. 8) according to the widths of the Cu patterns. As shown in Fig. 8, as the width of the pattern increased from 50 to 1000- μm with a fixed interval (50- μm), the maximum temperature increased from 500.6 to 590.8 $^{\circ}\text{C}$. Comparing the simulation results with the SEM analysis image (Fig. 6j), it seems that Cu nano/micro particles can be sintered at a temperature of 590.8 $^{\circ}\text{C}$. It can occur reasonably because the sintering of the copper nanoparticles proceeds before reaching to melting point, and the surface energy collapses due to the movement and resonance of atoms at the junctions between the particles [52, 53]. The generated heat accumulates in the copper electrode and rises in temperature without escaping to the PI substrate. In addition, since

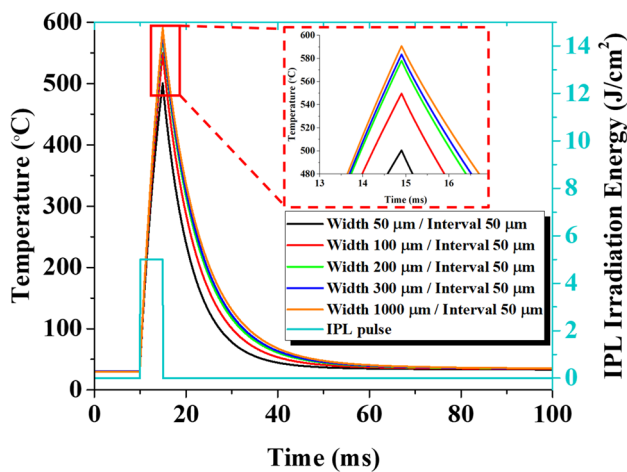


Fig. 8 Temperature distributions of the Cu patterns which have same interval of 50 μm and different widths (50, 100, 200, 300, 1000 μm)

the FLS program is a numerical computational program, it cannot reproduce the plasmonic behavior of copper nanoparticles or the motion of electrons and atoms. Therefore, in order to check the tendency of heat generation, the properties of the bulk copper were used, which may be different from the actual temperature. For that reason, it can occur reasonably because the sintering of the copper nanoparticles proceeds before reaching to melting point, and the surface energy collapses due to the movement and resonance of atoms at the junctions between the particles. Because of this, a strong resonance between electrons occurs between the surfaces of the nanoparticles, through which the surfaces of the copper particles melt and sinter.

To understand the in-depth mechanisms of the different temperature history from the pattern dimensions, the thermal distributions of three extreme pattern dimensions were calculated using the FLS and are plotted in Fig. 9a. The same IPL energy (5 J/cm^2) was irradiated onto the 3 cases of the Cu paste patterns. The temperature distributions at three different time points t_1 (12.5 ms), t_2 (15 ms), t_3 (17.5 ms) were plotted and shown in Fig. 9b. During the simulation, it was assumed that the IPL was absorbed by only the Cu paste patterns and generated heat. Heat generation in PI substrate was assumed to be negligible because the polyimide film absorbs UV near the 300 nm wavelength region [54, 55]. As shown in Fig. 9c, at the time of t_1 , heat was generated in each printed Cu electrode part, and dissipated to the nearby polyimide substrate. It is worth noting that, in Cases 2 and 3, the heat cannot be dissipated as quickly as in Case 1. This phenomenon is clearer in Case 3, where the width of the pattern is 1000- μm , and it is likely that the intervals among the patterns in Case 2 were all filled with Cu patterns. In Case 3, the heat from the printed Cu pattern was dissipated only at the two ends of the electrode, and thus the temperature of

the Cu pattern increased more quickly and reached a higher level (see Case 3 at t_1 (12.5 ms) in Fig. 9c). At the end time of the IPL irradiation at t_2 , in Case 3, the maximum temperature was 590.8 $^{\circ}\text{C}$, which is much higher than in the other Cases (Case 1, 489.1 $^{\circ}\text{C}$; Case 2, 500.6 $^{\circ}\text{C}$). The temperature difference remained the same even after the IPL irradiation. Note that, at the time of t_3 , the temperature of the Cu pattern in Case 3 was cooled down more slowly than in the other Cases and remained higher (444.4 $^{\circ}\text{C}$) (Case 1, 332.2 $^{\circ}\text{C}$; Case 2, 344.4 $^{\circ}\text{C}$).

The heat generated by the surface plasmonic effect is proportional to the area of the copper pattern. Therefore, the highest temperature is observed in Case 3, which has the largest copper electrode per unit area. The generated heat accumulates inside the copper electrode having high thermal conductivity (401 W/m K), and slowly escapes to the PI substrate having low thermal conductivity (0.12 W/m K). In addition, the heat dissipated to the PI substrate can be transferred to adjacent patterns because the interval between the patterns is very narrow. Therefore, the wider the width of the pattern and the narrower the interval of the pattern, the temperature increases the most during IPL sintering. On the other hand, the generated heat is discharged through the PI substrate for thermal equilibrium after finishing IPL irradiation. In Case 1, the electrode area is the smallest in the unit area. The amount of generated heat is relatively small, and the heat does not accumulate inside the copper electrode and escapes to the PI substrate. The heat dissipated through the PI substrate is easily reduced because there are no adjacent electrodes around it. Therefore, the narrower the width of the pattern and the wider the interval of the pattern, the temperature increase the least during IPL sintering.

3.3 Demonstrations for IPL Sintering Tendency

The phenomena mentioned above were verified through an in situ resistance monitoring experiment. For the experiment, the three most extreme cases among the cases mentioned above were determined (Case 1, the narrowest width of 50- μm and the widest interval of 1000- μm ; Case 2, the narrowest width of 50- μm and the narrowest interval of 50- μm ; and Case 3, the widest width of 1000- μm and the narrowest interval of 50- μm), as shown in Table 2. To measure the temperature of the pattern simultaneously during the IPL sintering process, in situ temperature monitoring was applied in previous studies [35, 56]. However, in this study, the pattern width was narrower than the thermocouple, which has a diameter of 200- μm , and thus the temperature monitoring was not possible. For this reason, instead of in situ temperature monitoring, in situ resistance monitoring was conducted to check the change in resistance during IPL sintering. To measure the resistance of the various sizes of the Cu patterns, 5 mm of both ends of

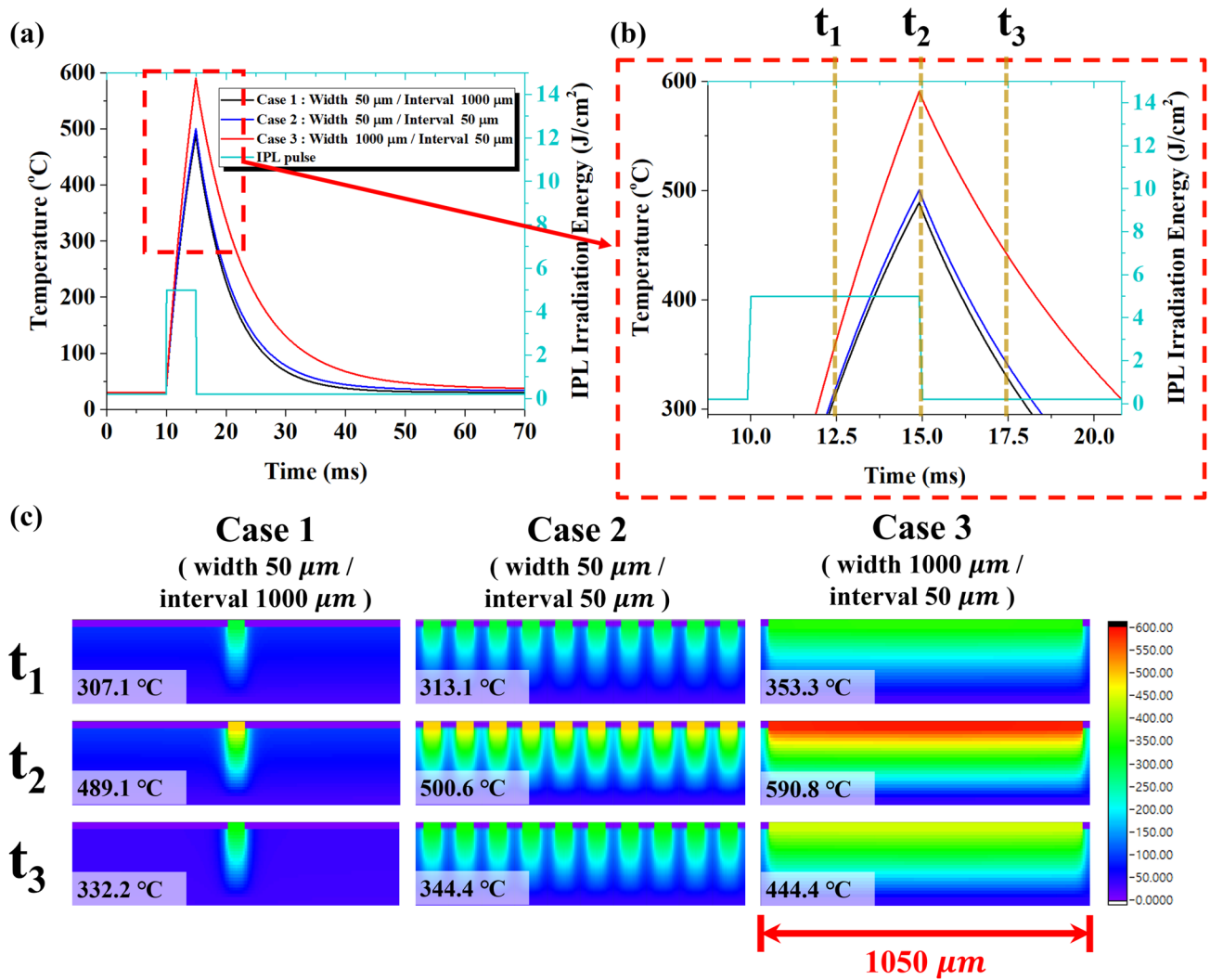


Fig. 9 a Heat generation on the Cu electrodes in 3 Cases with time scale. b Expanded figure of peak point of Case 1, 2 and 3 with specific time point t_1 (12.5 ms), t_2 (15 ms), and t_3 (17.5 ms). c 2-dimensional temperature distribution and maximum temperature of the

Cu electrodes of Case 1, Case 2, and case 3 in standard length of 1050 μm when the temperature is rising ($t_1=12.5$ ms), is maximum ($t_2=15$ ms), and is decreasing ($t_3=17.5$ ms)

the patterns were first sintered, and a silver paste was then applied followed by Cu tape. The silver paste decreased the contact resistance between the Cu pattern and the Cu tape (Fig. 10a). A Wheatstone bridge circuit was used and connected to the oscilloscope. Figure 10b shows the in situ

resistance monitoring results. Before the IPL irradiation, all three cases showed infinite resistance. The resistance was suddenly decreased once the IPL was irradiated. In all three cases, the reduction rate of the resistance differed despite the same IPL conditions (a single pulse, 5 J/cm² of energy, and a duration of 5 ms), which is consistent with the experiment and simulation results. The resistance of Case 3 (the widest electrode width of 1000-μm and narrowest interval of 50-μm) decreased the most, demonstrating the lowest resistivity, owing to its largest heat absorption area (the widest pattern width) by the IPL as well as the smallest heat spreading area (the narrowest interval). By contrast, Case 1 with the narrowest electrode width (50-μm) and widest interval (1000-μm) showed the highest resistivity owing to the smallest heat generation area by

Table 2 Three extreme conditions of the copper patterns which have different widths and intervals, resistivity and heat generation

	Case 1	Case 2	Case 3
Width (μm)	50	50	1000
Interval (μm)	1000	50	50
Resistivity (μΩ cm)	44.75	31.05	11.36
Temperature (°C)	489.1	500.6	590.8

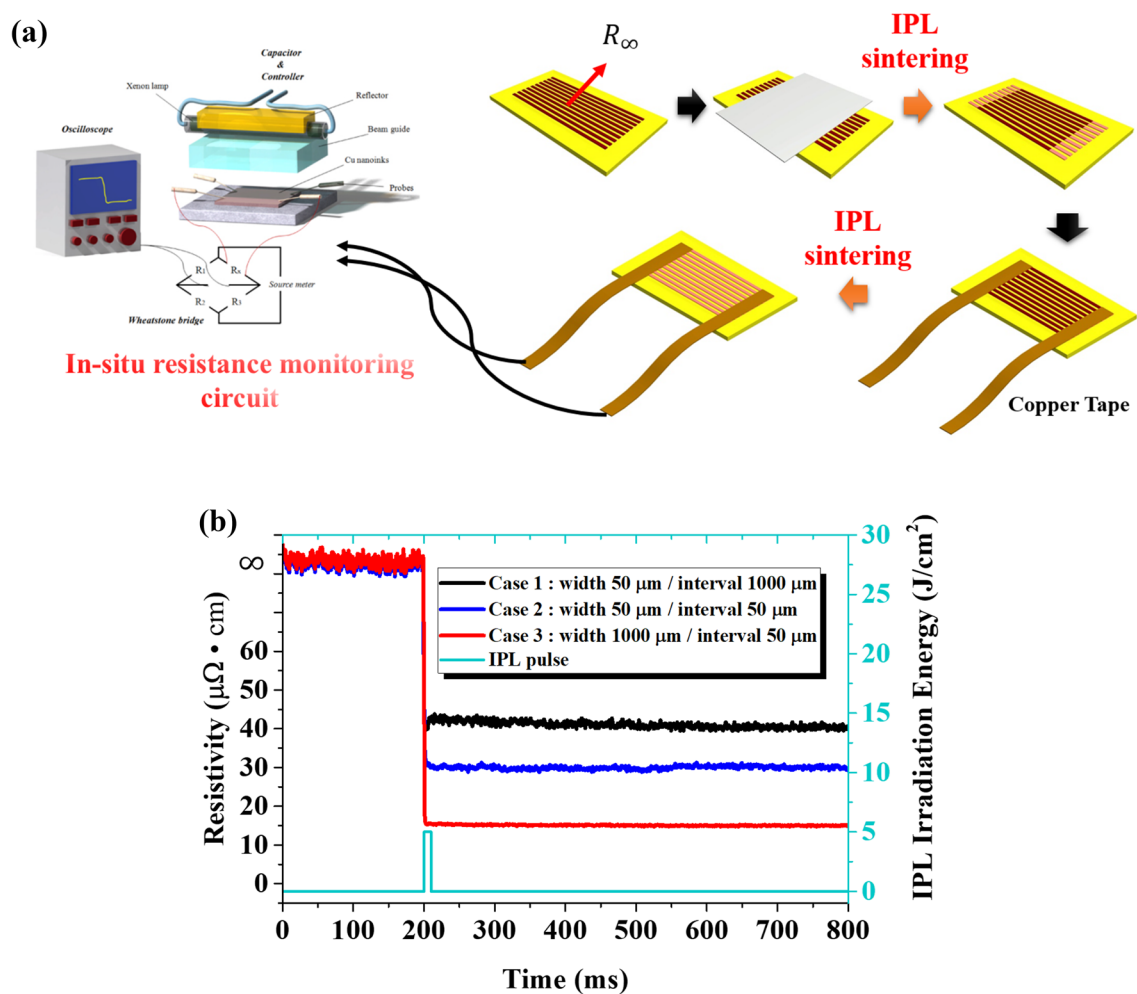


Fig. 10 **a** Fabricating 10 lines of Cu pattern specimens for in situ resistance monitoring, **b** In-situ resistance monitoring results of three Cases of Cu patterns with same IPL irradiation energy (5 J/cm^2)

the IPL with the largest heat spreading area. The in situ resistance monitoring results clearly show the effects of the pattern dimensions on the sintering behavior of the Cu patterns, derived from the fact that the increased heating and temperature by the IPL are dependent on the pattern width (the heat absorption and generation area by the IPL) and the pattern interval (the heat spreading area between patterns).

The predicted maximum temperatures of the Cu pattern with respect to the pattern widths and intervals are shown in Fig. 11. The temperature calculated using the FLS program showed almost the opposite tendency as the resistivity (see Fig. 4a, and for comparison, Fig. 11), which is reasonable because the lower resistivity indicates that the sintering was sufficient owing to the higher sintering temperature at the same IPL irradiation energy. Therefore, it can be concluded that the wider width of the patterns and the narrower intervals can induce a higher heat generation with the same IPL irradiation inducing a higher sintering temperature.

Therefore, the IPL sintering condition should be carefully designed by considering the pattern dimensions.

Unfortunately, in a real application, multi-sized pattern might be needed essentially in one electrodes. In this case, the IPL sintering conditions cannot be controlled in each patterns at the same time. Thus, in this study, the concept of dummy patterns was newly proposed for the uniform sintering degree on the different sizes of the Cu electrodes. To show the applicability of the dummy pattern concept, a digitizer pattern was applied. A digitizer is a large-sized printed electrode pattern, which is used for the touch panel of a smartphone or tablet PC. The digitizer electrode consisted of various sized patterns, as shown in Fig. 12b. Three patterns with a line width of $200\text{-}\mu\text{m}$ and intervals of $50\text{-}\mu\text{m}$ were applied, and these pattern bundles were separated using a 2-mm spacing. After the IPL sintering process, the patterns were not sufficiently sintered and the uniformity was poor under IPL irradiation conditions of a 5-ms pulse duration, a single pulse, and 5 J/cm^2 of energy. Observed using an

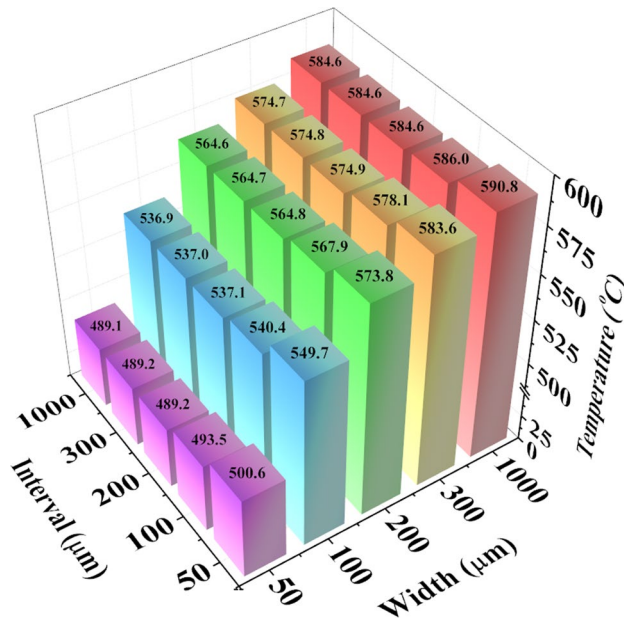


Fig. 11 Heat generation temperature after IPL irradiation (5 J/cm^2) followed by pattern intervals and widths using FLS program calculation

optical microscope, the polymer binders were not sufficiently removed and the Cu electrodes were delaminated (Fig. 12c). In addition, it was found that in a sparsely patterned area, the pattern was not sintered at all. It occurred because heat generation was insufficient for complete removal of the polymer binder with the IPL irradiation owing to the small pattern area. This phenomenon caused a thermal imbalance between the pattern and substrate and induced a delamination of the electrodes and a warpage of the entire printed circuit board. To solve this problem, a dummy pattern which is not related to the actual electrical circuit was printed between the pattern bundles (Fig. 12a). The dummy patterns were added

to the original patterns in the sparsely patterned areas, and the IPL sintering was conducted under same conditions as before. As a result, all patterns could be sintered sufficiently (the color of the entire Cu pattern was shiny pink owing to the sufficient sintering) without damage, delamination, or warpage of the PI substrate (Fig. 12e). In addition, the uniform line resistance (22.41Ω for 74 cm of an electric circuit with a width of $50\text{-}\mu\text{m}$) could be obtained in entire areas of the digitizer pattern.

4 Conclusions

In this study, the IPL sintering tendency according to the sizes of the copper pattern was demonstrated. When the pattern was the widest at $1000\text{-}\mu\text{m}$ and the narrowest at $50\text{-}\mu\text{m}$, it was expected that the highest heat was generated and the temperature increased to $590.8 \text{ }^\circ\text{C}$ calculated by FLS program. This high temperature effectively sintered the copper nano/micro particles, resulting in the lowest resistivity of $11.36 \mu\Omega \text{ cm}$. From experiment and simulation results, the narrower the width and the wider the interval, the less heat was generated, and the resistance reduction rate tends to be lowered. The heat generation database according to the dimension of the pattern was obtained through FLS program and compared with IPL sintering tendency. A dummy pattern was inserted between the digitizer electrodes printed with multi-sized pattern to generate the same heat in all regions during IPL sintering. When IPL sintered with the dummy patterns, the uniform line resistance (22.41Ω for 74 cm of an electric circuit with a width of $50\text{-}\mu\text{m}$) were measured in entire areas of the digitizer pattern. If it is possible to calculate the heat generation temperature according to the sizes of the Cu pattern, it was proved that uniform sintering of electrodes with multi-sized pattern.

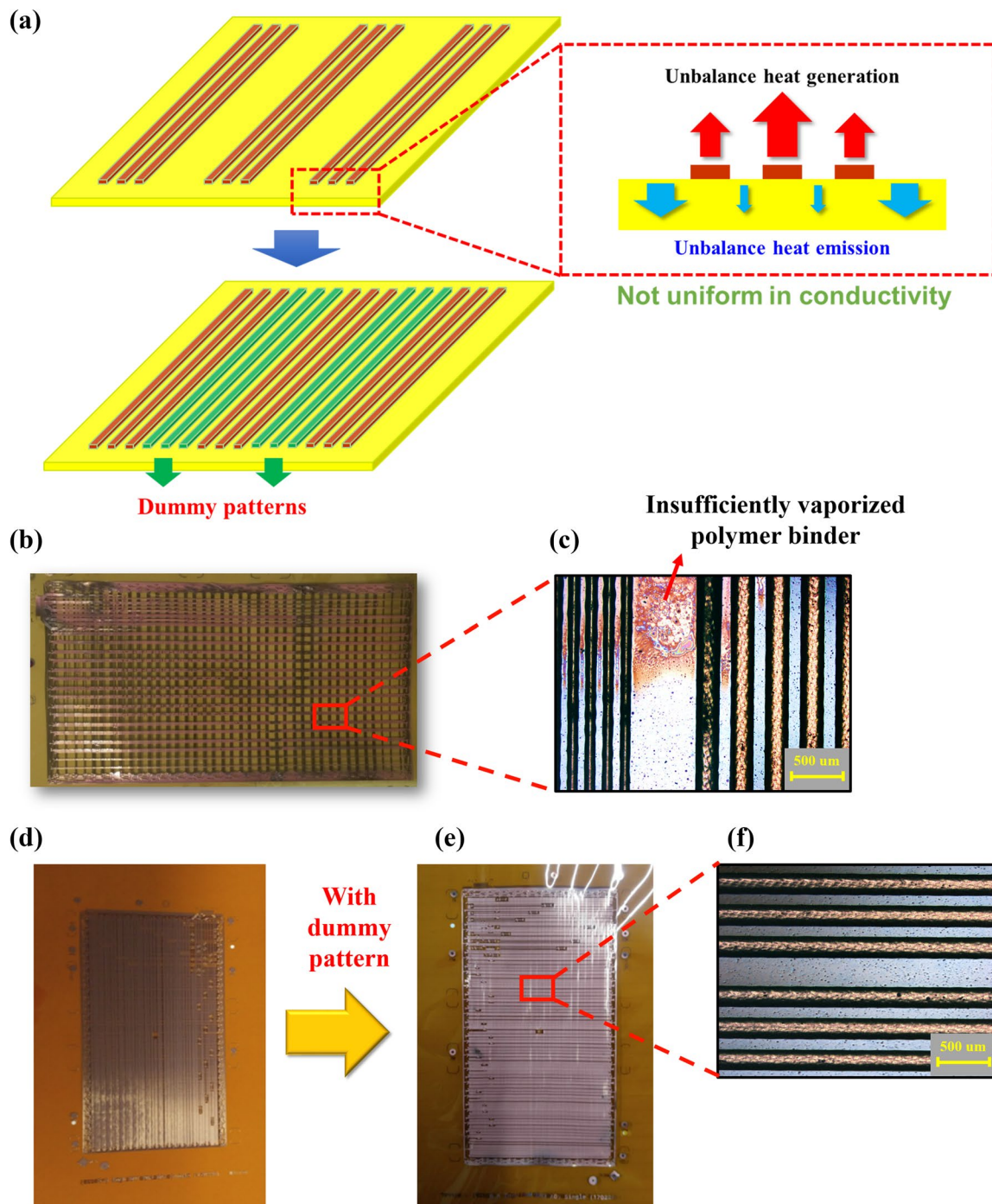


Fig. 12 **a** Concept schematic of the dummy patterns. **b** Image of original Digitizer pattern sintered by IPL irradiation, **c** expanded by optical microscope. **d** Image of new Digitizer patterns with dummy pattern before sintering, **e** after sintering, **f** expanded by optical microscope

Acknowledgements This work was supported by a National Research Foundation of Korea (NRF), funded by the Ministry of Education (2012R1A6A1029029, 2018R1D1A1A09083236). This work was also supported by Materials & Components Technology Development Program (20002957, Development of AgNW/rGO transparent electrode material and process based on IPL for OPV) funded by the Ministry of Trade, Industry & Energy (MOTIE, Korea).

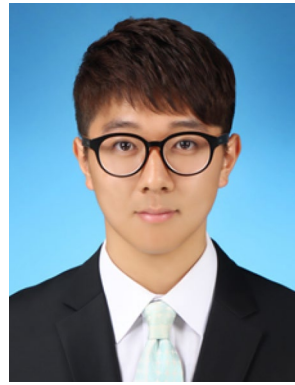
References

- Comiskey, B., Albert, J. D., Yoshizawa, H., & Jacobson, J. (1998). An electrophoretic ink for all-printed reflective electronic displays. *Nature*, 394, 253.

2. Zyung, T., Kim, S. H., Chu, H. Y., Lee, J. H., Lim, S. C., Lee, J.-I., et al. (2005). Flexible organic LED and organic thin-film transistor. *Proceedings of the IEEE*, *93*, 1265–1272.
3. Kondo, Y., Tanabe, H., & Otake, T. (2010). Novel electrochromic polymer for electronic paper. *IEICE Transactions on Electronics*, *93*, 1602–1606.
4. Yang, Y., & Heeger, A. (1994). Polyaniline as a transparent electrode for polymer light-emitting diodes: Lower operating voltage and higher efficiency. *Applied Physics Letters*, *64*, 1245–1247.
5. Haight, R. A., & Troutman, R. R. (1998). Optically transparent diffusion barrier and top electrode in organic light emitting diode structures, in Google Patents.
6. Leem, D. S., Edwards, A., Faist, M., Nelson, J., Bradley, D. D., & de Mello, J. C. (2011). Efficient organic solar cells with solution-processed silver nanowire electrodes. *Advanced Materials*, *23*, 4371–4375.
7. Zou, J., Yip, H.-L., Hau, S. K., & Jen, A. K.-Y. (2010). Metal grid/conducting polymer hybrid transparent electrode for inverted polymer solar cells. *Applied Physics Letters*, *96*, 96.
8. Subramanian, V., Fréchet, J. M., Chang, P. C., Huang, D. C., Lee, J. B., Moles, S. E., et al. (2005). Progress toward development of all-printed RFID tags: materials, processes, and devices. *Proceedings of the IEEE*, *93*, 1330–1338.
9. Bansal, R. (2003). Coming soon to a Wal-Mart near you. *IEEE Antennas and Propagation Magazine*, *45*, 105–106.
10. Jost, K., Stenger, D., Perez, C. R., McDonough, J. K., Lian, K., Gogotsi, Y., et al. (2013). Knitted and screen printed carbon-fiber supercapacitors for applications in wearable electronics. *Energy and Environmental Science*, *6*, 2698–2705.
11. Yeo, J., Kim, G., Hong, S., Kim, M. S., Kim, D., Lee, J., et al. (2014). Flexible supercapacitor fabrication by room temperature rapid laser processing of roll-to-roll printed metal nanoparticle ink for wearable electronics application. *Journal of Power Sources*, *246*, 562–568.
12. Hecht, D. S., Thomas, D., Hu, L., Ladous, C., Lam, T., Park, Y., et al. (2009). Carbon-nanotube film on plastic as transparent electrode for resistive touch screens. *Journal of the Society for Information Display*, *17*, 941–946.
13. Madaria, A. R., Kumar, A., & Zhou, C. (2011). Large scale, highly conductive and patterned transparent films of silver nanowires on arbitrary substrates and their application in touch screens. *Nanotechnology*, *22*, 245201.
14. Deng, D., Jin, Y., Cheng, Y., Qi, T., & Xiao, F. (2013). Copper nanoparticles: aqueous phase synthesis and conductive films fabrication at low sintering temperature. *ACS Applied Materials and Interfaces*, *5*, 3839–3846.
15. Kang, H., Sowade, E., & Baumann, R. R. (2014). Direct intense pulsed light sintering of inkjet-printed copper oxide layers within six milliseconds. *ACS Applied Materials and Interfaces*, *6*, 1682–1687.
16. Greer, J. R., & Street, R. A. (2007). Thermal cure effects on electrical performance of nanoparticle silver inks. *Acta Materialia*, *55*, 6345–6349.
17. Yu, J. H., Rho, Y., Kang, H., Jung, H. S., & Kang, K.-T. (2015). Electrical behavior of laser-sintered Cu based metal-organic decomposition ink in air environment and application as current collectors in supercapacitor. *International Journal of Precision Engineering and Manufacturing-Green Technology*, *2*, 333–337.
18. Yu, J. H., Kang, K.-T., Hwang, J. Y., Lee, S.-H., & Kang, H. (2014). Rapid sintering of copper nano ink using a laser in air. *International journal of Precision Engineering and Manufacturing*, *15*, 1051–1054.
19. Allabergenov, B., & Kim, S. (2013). Investigation of electro-physical and mechanical characteristics of porous copper-carbon composite materials prepared by spark plasma sintering. *International Journal of Precision Engineering and Manufacturing*, *14*, 1177–1183.
20. Wünscher, S., Abbel, R., Perelaer, J., & Schubert, U. S. (2014). Progress of alternative sintering approaches of inkjet-printed metal inks and their application for manufacturing of flexible electronic devices. *Journal of Materials Chemistry C*, *2*, 10232–10261.
21. Ma, J., Diehl, J., Johnson, E., Martin, K., Miskovsky, N., Smith, C., et al. (2007). Systematic study of microwave absorption, heating, and microstructure evolution of porous copper powder metal compacts. *Journal of Applied Physics*, *101*, 074906.
22. Sung, K.-H., Park, J., & Kang, H. (2018). Multi-layer inkjet printing of Ag nanoparticle inks and its sintering with a near-infrared system. *International Journal of Precision Engineering and Manufacturing*, *19*, 303–307.
23. Kinney, L. C., & Tompkins, E. H. (1969). Method of making printed circuits, in U.S..
24. Matsumoto, K., Sakoda, T., Nasu, M., & Ikeda, G. (2008). Film deposition method and film deposition system, in U.S.
25. Hirai, S. K. K. (2002). Conductive path or electrode, and method for forming the same, in Japan.
26. Dharmadasa, R., Jha, M., Amos, D. A., & Druffel, T. (2013). Room temperature synthesis of a copper ink for the intense pulsed light sintering of conductive copper films. *ACS Applied Materials and Interfaces*, *5*, 13227–13234.
27. Patil, S. A., Ryu, C.-H., & Kim, H.-S. (2018). Synthesis and characterization of copper nanoparticles (Cu-Nps) using rongalite as reducing agent and photonic sintering of Cu-Nps ink for printed electronics. *International Journal of Precision Engineering and Manufacturing-Green Technology*, *5*, 239–245.
28. Araki, T., Sugahara, T., Jiu, J., Nagao, S., Nogi, M., Koga, H., et al. (2013). Cu salt ink formulation for printed electronics using photonic sintering. *Langmuir*, *29*, 11192–11197.
29. Wong, D., Yim, C., & Park, S. S. Hybrid manufacturing of oxidation resistant cellulose nanocrystals-copper-graphene nanoplatelets based electrodes. In *International journal of precision engineering and manufacturing-green technology*, pp. 1–15.
30. Schroder, K., McCool, S., & Furlan, W. (2006). Broadcast photonic curing of metallic nanoparticle films. *NSTI Nanotech*, *7*, 11.
31. Schroder, K. A., McCool, S., Hamill, D., Wilson, D., Furlan, W., Walter, K., Willauer, D., & Martin, K. (2010). Electrical, plating and catalytic uses of metal nanomaterial compositions, in U.S.
32. Kim, H.-S., Dhage, S. R., Shim, D.-E., & Hahn, H. T. (2009). Intense pulsed light sintering of copper nanoink for printed electronics. *Applied Physics A*, *97*, 791.
33. Han, Q., Sun, S., Li, J., & Wang, X. (2011). Growth of copper sulfide dendrites and nanowires from elemental sulfur on TEM Cu grids under ambient conditions. *Nanotechnology*, *22*, 155607.
34. Ryu, J., Kim, H.-S., & Hahn, H. T. (2011). Reactive sintering of copper nanoparticles using intense pulsed light for printed electronics. *Journal of Electronic Materials*, *40*, 42–50.
35. Joo, S.-J., Hwang, H.-J., & Kim, H.-S. (2014). Highly conductive copper nano/microparticles ink via flash light sintering for printed electronics. *Nanotechnology*, *25*, 265601.
36. Patil, S. A., Hwang, H.-J., Yu, M.-H., Shrestha, N. K., & Kim, H.-S. (2017). Photonic sintering of a ZnO nanosheet photoanode using flash white light combined with deep UV irradiation for dye-sensitized solar cells. *RSC Advances*, *7*, 6565–6573.
37. Abdullah, E. C., & Geldart, D. (1999). The use of bulk density measurements as flowability indicators. *Powder Technology*, *102*, 151–165.
38. Ryu, C.-H., Moon, C.-J., & Kim, H.-S. (2019). A study on the relationship between print-ability and flash light sinter-ability of

- Cu nano/micro-ink for printed electronics. *Thin Solid Films*, 671, 36–43.
39. Lin, H.-W., Chang, C.-P., Hwu, W.-H., & Ger, M.-D. (2008). The rheological behaviors of screen-printing pastes. *Journal of Materials Processing Technology*, 197, 284–291.
 40. Hwang, H.-J., Oh, K.-H., & Kim, H.-S. (2016). All-photonics drying and sintering process via flash white light combined with deep-UV and near-infrared irradiation for highly conductive copper nano-ink. *Scientific Reports*, 6, 19696.
 41. Hwang, H.-J., Chung, W.-H., & Kim, H.-S. (2012). In situ monitoring of flash-light sintering of copper nanoparticle ink for printed electronics. *Nanotechnology*, 23, 485205.
 42. Hwang, Y.-T., Chung, W.-H., Jang, Y.-R., & Kim, H.-S. (2016). Intensive plasmonic flash light sintering of copper nanoinks using a band-pass light filter for highly electrically conductive electrodes in printed electronics. *ACS Applied Materials and Interfaces*, 8, 8591–8599.
 43. Yim, C., Greco, K., Sandwell, A., & Park, S. S. (2017). Eco-friendly and rapid fabrication method for producing polyethylene terephthalate (PET) mask using intensive pulsed light. *International Journal of Precision Engineering and Manufacturing-Green Technology*, 4, 155–159.
 44. Ryu, C.-H., Joo, S.-J., & Kim, H.-S. (2019). Intense pulsed light sintering of Cu nano particles/micro particles-ink assisted with heating and vacuum holding of substrate for warpage free printed electronic circuit. *Thin Solid Films*, 675, 23–33.
 45. Cengel, A. (2007). HEHT transfer.
 46. Soares, D., Jr., & Wrobel, L. C. (2019). A locally stabilized explicit approach for nonlinear heat conduction analysis. *Computers and Structures*, 214, 40–47.
 47. Agarwala, M., Bourell, D., Beaman, J., Marcus, H., & Barlow, J. (1995). Direct selective laser sintering of metals. *Rapid Prototyping Journal*, 1, 26–36.
 48. El-Sayed, M. A. (2001). Some interesting properties of metals confined in time and nanometer space of different shapes. *Accounts of Chemical Research*, 34, 257–264.
 49. Link, S., & El-Sayed, M. A. (2000). Shape and size dependence of radiative, non-radiative and photothermal properties of gold nanocrystals. *International Reviews in Physical Chemistry*, 19, 409–453.
 50. Hartland, G. V. (2006). Coherent excitation of vibrational modes in metallic nanoparticles. *Annual Review of Physical Chemistry*, 57, 403–430.
 51. Chung, W.-H., Hwang, H.-J., & Kim, H.-S. (2015). Flash light sintered copper precursor/nanoparticle pattern with high electrical conductivity and low porosity for printed electronics. *Thin Solid Films*, 580, 61–70.
 52. German, R. M. (1996). Sintering theory and practice. In *Solar-Terrestrial Physics*, p. 568.
 53. Shatokha, V. (2012). Sintering: Methods and products, BoD-books on demand.
 54. Damaceanu, M.-D., Rusu, R.-D., Bruma, M., & Jarzabek, B. (2010). Photo-optical properties of poly (oxadiazole-imide) s containing naphthalene rings. *Polymer Journal*, 42, 663.
 55. Kim, D., & Shen, Y. (1999). Study of wet treatment of polyimide by sum-frequency vibrational spectroscopy. *Applied Physics Letters*, 74, 3314–3316.
 56. Park, S.-H., Chung, W.-H., & Kim, H.-S. (2014). Temperature changes of copper nanoparticle ink during flash light sintering. *Journal of Materials Processing Technology*, 214, 2730–2738.

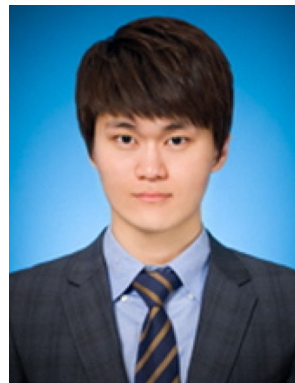
Publisher's Note Springer Nature remains neutral with regard to jurisdictional claims in published maps and institutional affiliations.



Yong-Rae Jang is currently a Ph.D. Candidate in the Department of Mechanical Engineering at Hanyang University in South Korea. His research interests include printed electronics, transparent electrodes, and semiconductor manufacturing & packaging technology.



Chung-Hyeon Ryu received his Master's degree in the Department of Mechanical Engineering at Hanyang University in South Korea in 2015. He also received his Ph.D. degree of the Department of Mechanical Engineering at Hanyang University in South Korea in 2019. His research interests include printed electronics, solar cells, and semiconductor manufacturing & packaging technology.



Yeon-Taek Hwang is currently a Ph.D. Candidate in the Department of Mechanical Engineering at Hanyang University in South Korea. His research interests include printed electronics, composite modeling and nuclear fuel performance.



Hak-Sung Kim is a professor in the Department of Mechanical Engineering at Hanyang University in South Korea since 2010. His research interests include structural composite, printed electronics, nondestructive evaluation with terahertz and semiconductor packaging technology.